Supporting Information for

Counting secondary loops is required for accurate prediction of end-linked polymer network elasticity

Junpeng Wang,[†] Tzyy-Shyang Lin,[‡] Yuwei Gu,[†] Rui Wang,[‡] Bradley D. Olsen,[‡]* Jeremiah A. Johnson[†]*

[†]Department of Chemistry, Massachusetts Institute of Technology, Cambridge, MA 02139

[‡]Department of Chemical Engineering, Massachusetts Institute of Technology, Cambridge, MA 02139

Correspondence to: jaj2109@mit.edu (JAJ) and bdolsen@mit.edu(BDO)

Table of Contents

1. The equations to calculate $n_{1,3}$ and $n_{2,3}$ from measured mass distributions

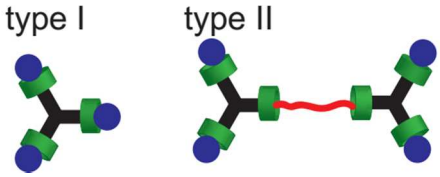

Type I and type II junctions are the two types of junctions whose mass distributions can be measured to afford the nominal primary loop fractions $n_{1,3*}$ and $n_{1,4*}$. In order to relate $n_{1,3*}$ and $n_{1,4*}$ to the actual primary ($n_{1,3}$) and secondary loop ($n_{2,3}$) fractions, the abundances of all of the trifunctional junctions are analyzed. Let the fraction of the nondegradable macromer be y, the number of typical 1° loop per type II junction be m_1, and number of 2° loop per type II junction be m_2. Table S1 lists the abundance of all of the trifunctional junctions (a-h).

Table S1. The abundance of different trifunctional junctions.

Ideal	Fraction of junctions	1° loop	Fractions of junctions
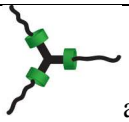 a	$(1-n_{1,3})(1-y)^3$	 b	$n_{1,3}(1-y)^2$
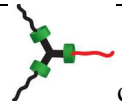 c	$3(1-n_{1,3})y(1-y)^2$	 d	$n_{1,3}y(1-y)$
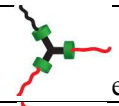 e	$3(1-n_{1,3})y^2(1-y)$	 f	$n_{1,3}y(1-y)$
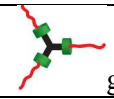 g	$(1-n_{1,3})y^3$	 h	$n_{1,3}y^2$

$n_{1,3*}$ can be can calculated from the following equation based on the mass distribution of type I junctions[1-2]: $\frac{[iii]}{[nii]}=\frac{1+n_{1,3*}}{3-n_{1,3*}}$ (Eq. S1)

According to Table S1, type I has two possibilities: a and b.

$$n_{1,3*}=\frac{[b]}{[a]+[b]}=\frac{n_{1,3}(1-y)^2}{(1-n_{1,3})(1-y)^3+n_{1,3}(1-y)^2}=\frac{n_{1,3}}{(1-n_{1,3})(1-y)+n_{1,3}} \quad \text{(Eq. S2)}$$

From Eq. S2, $n_{1,3}=\frac{(1-y)n_{1,3*}}{1-yn_{1,3*}}$ (Eq. S3)

Eq. S3 highlights that the actual primary loop fraction ($n_{1,3}$) is not identical to the nominal one ($n_{1,3*}$), which is obtained by analyzing the mass distribution of type I junction, and they are quantitatively related by the fraction of nondegradable chain (y).

$n_{1,4*}$ can be can calculated from the following equation based on the mass distribution of type II junctions, similar to our previous work on the tetrafunctional junction networks[3]:

$$\frac{[iiii]}{[niii]}=\frac{2+n_{1,4*}}{4(2-n_{1,4*})} \quad \text{(Eq. S4)}$$

According to Table S1, the number of 1° loop per type II junction:

$m_1=\frac{2[d]}{[c]+[d]}=\frac{2n_{1,3}y(1-y)}{3(1-n_{1,3})y(1-y)^2+n_{1,3}y(1-y)}$ (Eq. S5) (The factor 2 is needed because there are 2 trifunctional junctions on a type II junction)

Number of 2° loop per type II junction: $m_2=n_{1,4*}-m_1$ (Eq. S6)

In order to convert the number of secondary loop per type II junction m_2 to the number of secondary loop per normal junction $n_{2,3}$, we look at a junction X that is connected to a nondegradable chain (Figure S1). Junction X has 3 junction points 1, 2 and 3. A type II junction connects 2 trifunctional junctions, and the measurement only involve the secondary loops formed by junction points 1&2 (Figure S1, left) and 1&3 (Figure 1, middle), but does not include the secondary loop formed by junction points 2&3 (Figure 1, right). Since the probability of 2° loops formed with junction points 1&2, 1&3 and 2&3 should be identical, the measured 2° loops formed at junction X will be the two thirds of the total 2° loops formed at junction X. The number of 2° loop per trifunctional junction, i.e., 2° loop fraction is

$n_{2,3}=\frac{1}{2}m_2\times\frac{3}{2}=\frac{3}{4}m_2$ (Eq. S7)

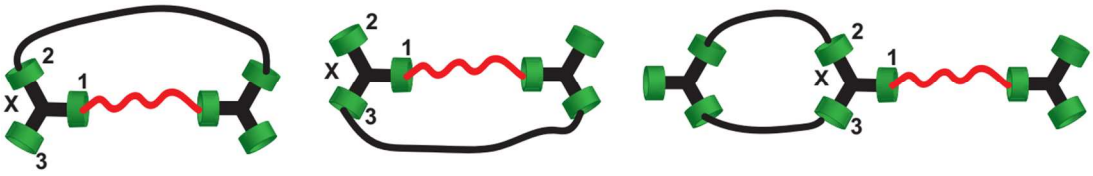

Figure S1. The possible secondary loops formed by junction X with three junction points 1, 2 and 3.

2. Materials and Methods

Unless otherwise mentioned, all reagents were purchased from Sigma-Aldrich and used without further purification. Monodisperse PEG12 and PEG28 diols were purchased from Polypure. 6-azido-2,2-dimethylhexanoic acid, 6-azido-2,2-dimethylhexanoic-3,3,4,4,5,5,6,6-d8 acid, and the tris-alkyne crosslinker $\mathbf{B_3}$ were synthesized by following our previously reported procedures.[3] 6-azidohexyl tosylate was synthesized by following literature procedure.[4] CuBr and Me_6TREN were purified according to previously reported procedures[3] and transferred into a N_2-filled glovebox before use.
Liquid chromatography–mass spectrometry (LC/MS) was performed on an Agilent 1260 LC system equipped with a Zorbax SB-C18 rapid resolution HT column and a Zorbax SB-C18 semi-preparative column. Solvent gradients consisted of mixtures of nano-pure H_2O with 0.1% acetic acid (AcOH) and HPLC-grade acetonitrile (MeCN). Mass spectra were obtained using an Agilent 6130 single quadrupole mass spectrometer. ^{1}H nuclear magnetic resonance (^{1}H NMR) and ^{13}C nuclear magnetic resonance (^{13}C-NMR) spectra were recorded on Bruker AVANCE-400 NMR spectrometers in the Department of Chemistry Instrumentation Facility at MIT. Chemical shifts are expressed in parts per million (ppm), and splitting patterns are designated as s (singlet), d (doublet), t (triplet), m (multiplet) and br (broad). Coupling constants J are reported in Hertz (Hz). High-resolution mass spectrometry (HRMS) was conducted with ElectroSpray Ionization (ESI) method on a Waters Qtof Premier instrument in the positive mode. The optimized condition was as follows: Capillary = 3000 kV, Cone = 35, Source Temperature = 120 °C and Desolvation Temperature = 350 °C. Preparative gel-permeation chromatography (prep-GPC) was performed on a JAI Preparative Recycling HPLC (LaboACE-LC-5060) system equipped with either 2.5HR and 2HR columns in series (20 mm ID x 600 mm length) or 2.5H and 2H columns in series (40 mm ID x 600 mm length) using $CHCl_3$ as the eluent.

3. Synthesis

$\mathbf{A_{2H}}$ (PEG-12)

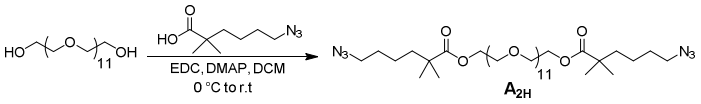

In a round-bottom flask, PEG-12 diol (5 g, 9.15 mmol, 1.0 eq) was dissolved in 50 mL dichloromethane. To the solution was added 6-azido-2,2-dimethylhexanoic acid (4.4 g, 23.8 mmol, 2.6 eq) and 4-dimethyl aminopyridine (1.12 g, 9.15 mmol, 1.0 eq). The solution was cooled down to 0 °C in an ice/water bath before (3-Dimethylaminopropyl)-N'-ethylcarbodiimide hydrochloride (7.02 g, 36.6 mmol, 4.0 eq) was added. The solution was allowed to warm to room temperature and stirred for 36 h. The reaction mixture was washed with water (2 × 100 mL) and brine (100 mL) and dried with magnesium sulfate. The solvent was removed under reduced pressure and the residue was purified with prep GPC and resulted in $\mathbf{A_{2H}}$ (PEG-12) as a light yellow liquid (7.66 g, yield: 95%). ^{1}H NMR (500 MHz, $CDCl_3$) δ 4.22 (t, J = 5.7 Hz, 4H), 3.68 (dd, J = 5.7, 4.1 Hz, 4H), 3.66 – 3.60 (m, 40H), 3.26 (t, J = 6.9 Hz, 4H), 1.58 – 1.50 (m, 8H), 1.37 – 1.24 (m, 4H), 1.18 (s, 12H). ^{13}C NMR (101 MHz, $CDCl_3$) δ 177.67, 77.48, 77.16, 76.84, 70.61,

70.60, 70.56, 69.18, 63.46, 51.23, 42.22, 40.04, 29.27, 25.13, 22.18. HRMS-ESI (m/z): calcd for $C_{40}H_{76}N_6O_{15}Na$ $[M+Na]^+$, 903.5261; found, 903.5258.

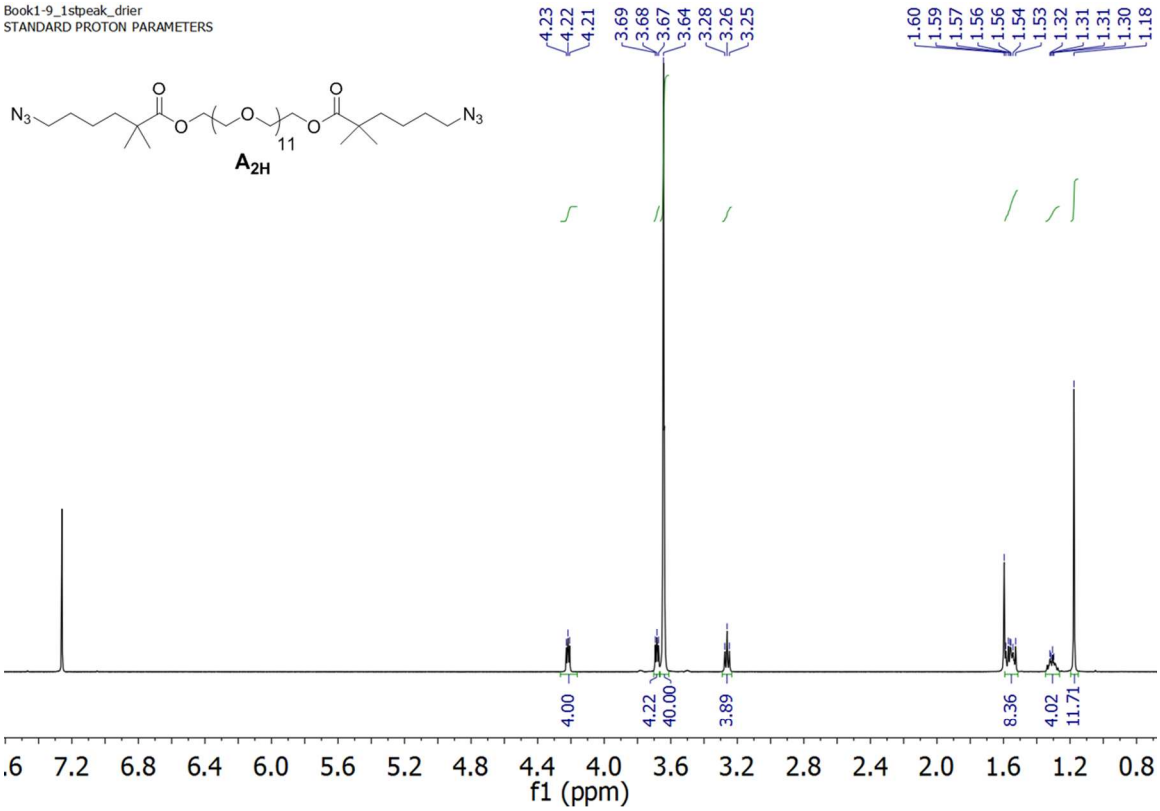

Figure S2. ^{1}H NMR (500 MHz, $CDCl_3$) for $\mathbf{A_{2H}}$ (PEG-12).

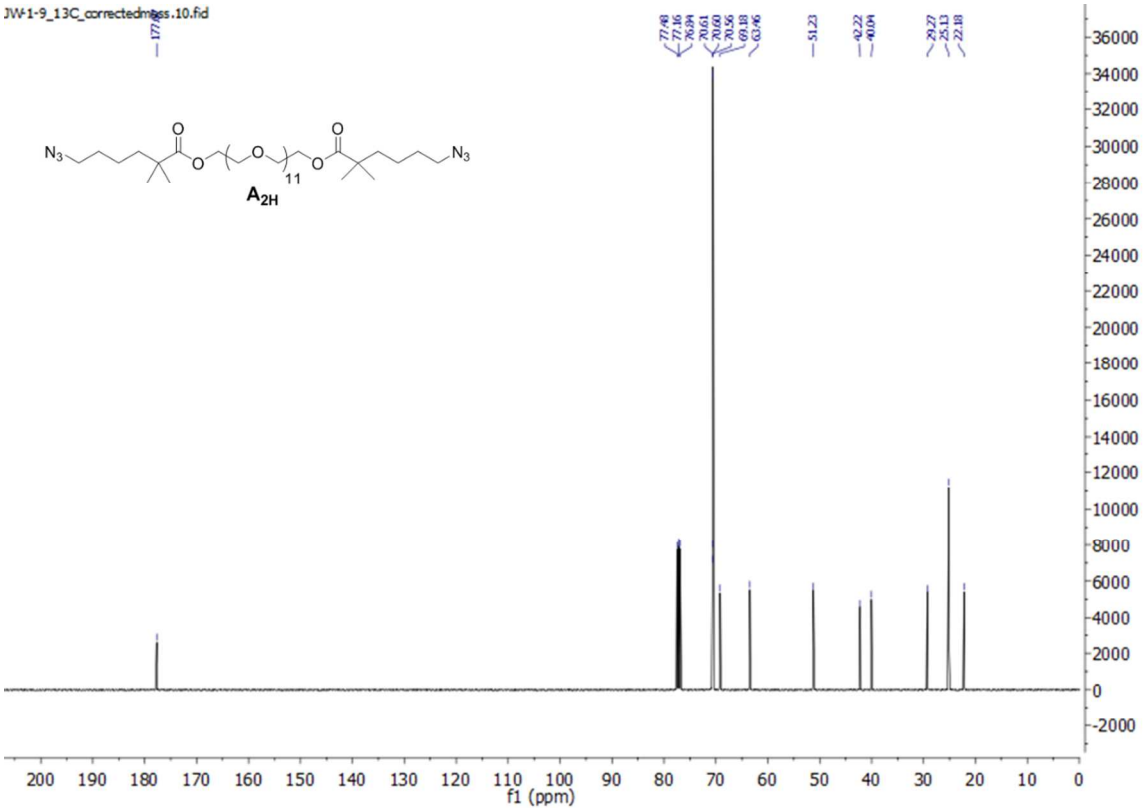

Figure S3. ^{13}C NMR (101 MHz, $CDCl_3$) for $\mathbf{A_{2H}}$ (PEG-12).

A_{2D} (PEG-12)

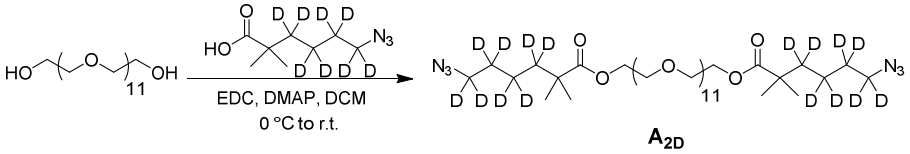

The synthesis of $\mathbf{A_{2D}}$ (PEG-12) was conducted using similar procedure as that of $\mathbf{A_{2H}}$ (PEG-12), except that 6-azido-2,2-dimethylhexanoic-3,3,4,4,5,5,6,6-d8 acid instead of the nonisotopic analogue was used. ^1H NMR (500 MHz, $CDCl_3$) δ 4.22 (t, J = 5.6 Hz, 4H), 3.68 (dd, J = 5.6, 4.3 Hz, 4H), 3.66 – 3.60 (m, 40H), 1.17 (s, 12H). ^{13}C NMR (101 MHz, $CDCl_3$) δ 177.80, 70.73, 70.71, 70.67, 70.65, 69.28, 63.54, 42.15, 25.16. The resonance for the deuterated carbons is absent due to the lack of dipolar relaxation and NOE enhancement, which result from the lack of protons. HRMS-ESI (m/z): calcd for $C_{40}H_{60}D_{16}N_6O_{15}Na$ $[M+Na]^+$, 919.6265; found, 919.6263.

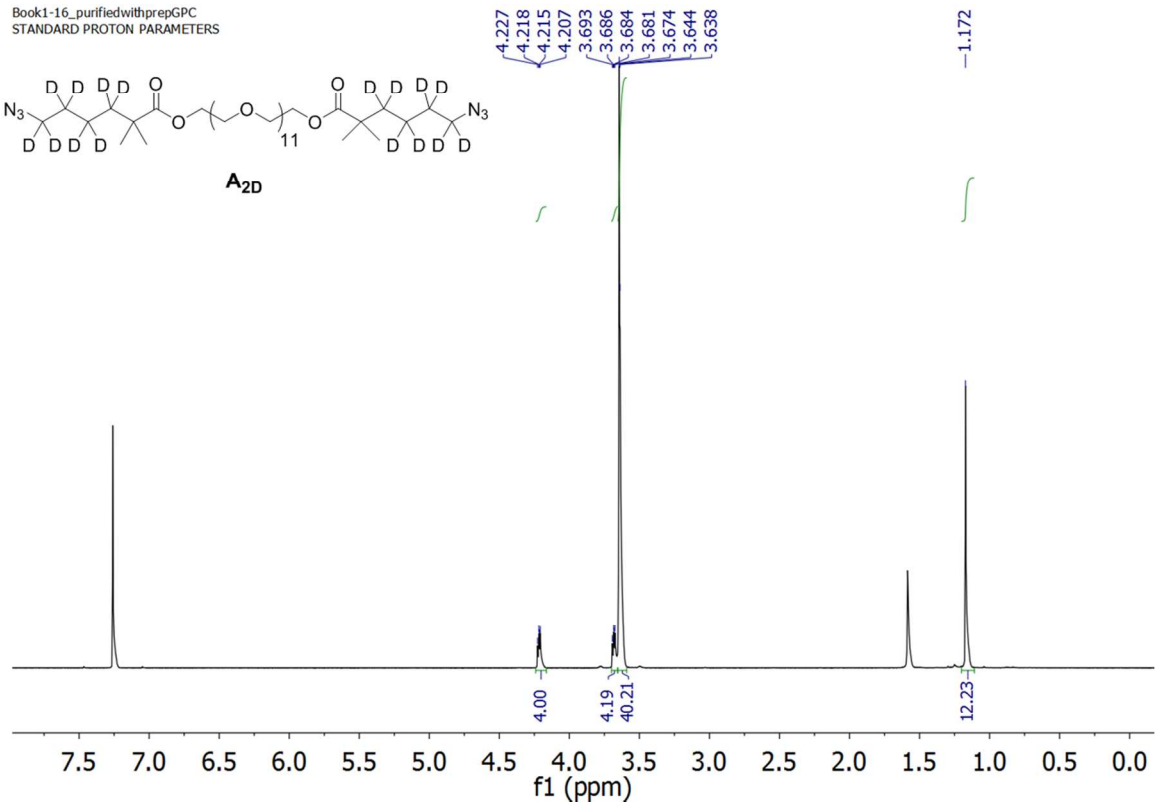

Figure S4. ^{1}H NMR (500 MHz, $CDCl_3$) for $\mathbf{A_{2D}}$ (PEG-12).

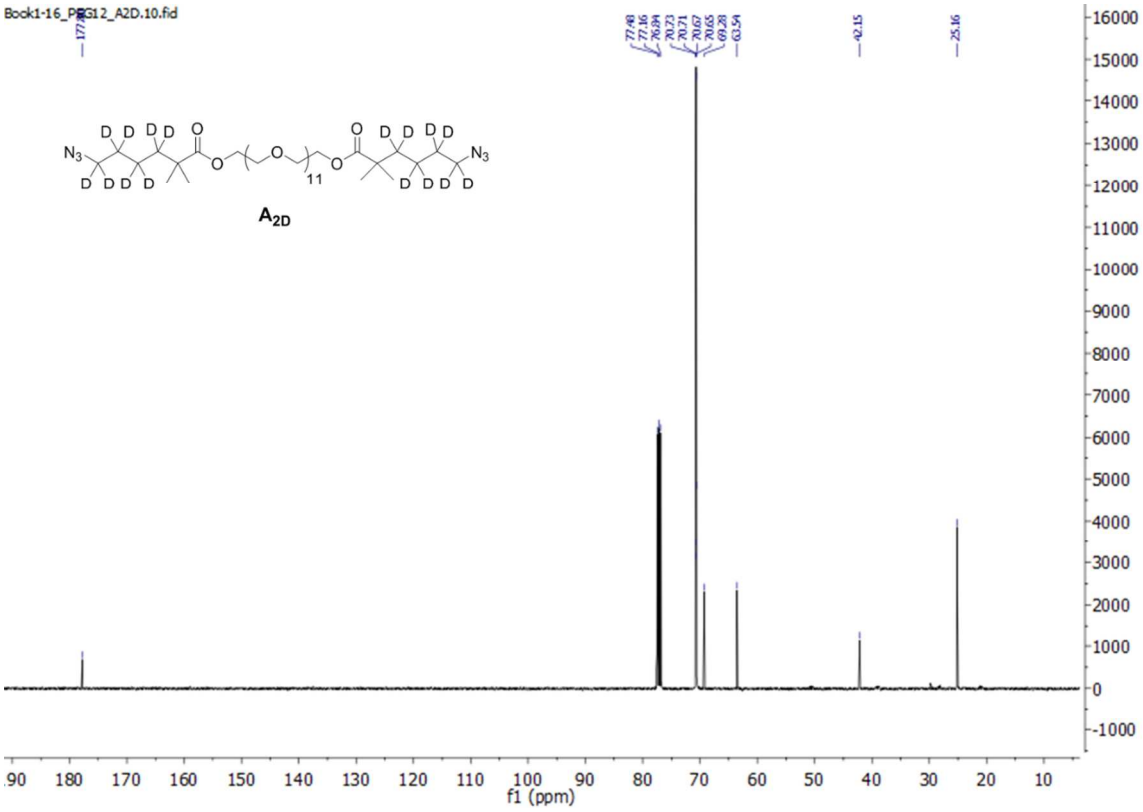

Figure S5. ^{13}C NMR (101 MHz, $CDCl_3$) for $\mathbf{A_{2D}}$ (PEG-12).

$\mathbf{A_{2N}}$ (PEG-12)

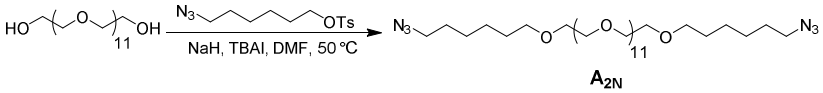

To a flame dried 2-neck 50 mL round bottle flask was added 60% NaH/mineral oil (0.044 g, 1.098 mmol), and 10 mL DMF under nitrogen, and to the mixture was added PEG-12 diol (0.3 g, 0.549 mmol). The mixture was stirred at 50 °C for 1 h before 6-azidohexyl tosylate (0.327 g, 1.098 mmol) and tetrabutylammonium iodide (0.020 g, 0.055 mmol) were added, and the reaction mixture was allowed to proceed under nitrogen at 50 °C for 24 h. Solvent was removed by rotary evaporation and water was added to dissolve the mixture. The solution was extracted with dichloromethane (20 mL × 3) and the combined organic layer was washed with brine and dried over Na_2SO_4. The crude product was purified with prep-GPC, affording light yellow oil as the product (0.35 g, yield: 80%). ^1H NMR (500 MHz, $CDCl_3$) δ 3.66-3.60 (m, 44H), 3.58 (t, J = 5.9, 4H), 3.46 (t, J = 6.6 Hz, 4H), 3.27 (t, J = 6.9 Hz, 4H), 1.66 – 1.51 (m, 8H), 1.47 – 1.29 (m, 8H). ^{13}C NMR (101 MHz, $CDCl_3$) δ 71.30, 70.70, 70.68, 70.66, 70.19, 51.47, 29.56, 28.88, 26.64, 25.78. HRMS-ESI (m/z): calcd for $C_{36}H_{72}N_6O_{13}Na$ $[M+Na]^+$, 797.5230; found, 797.5201.

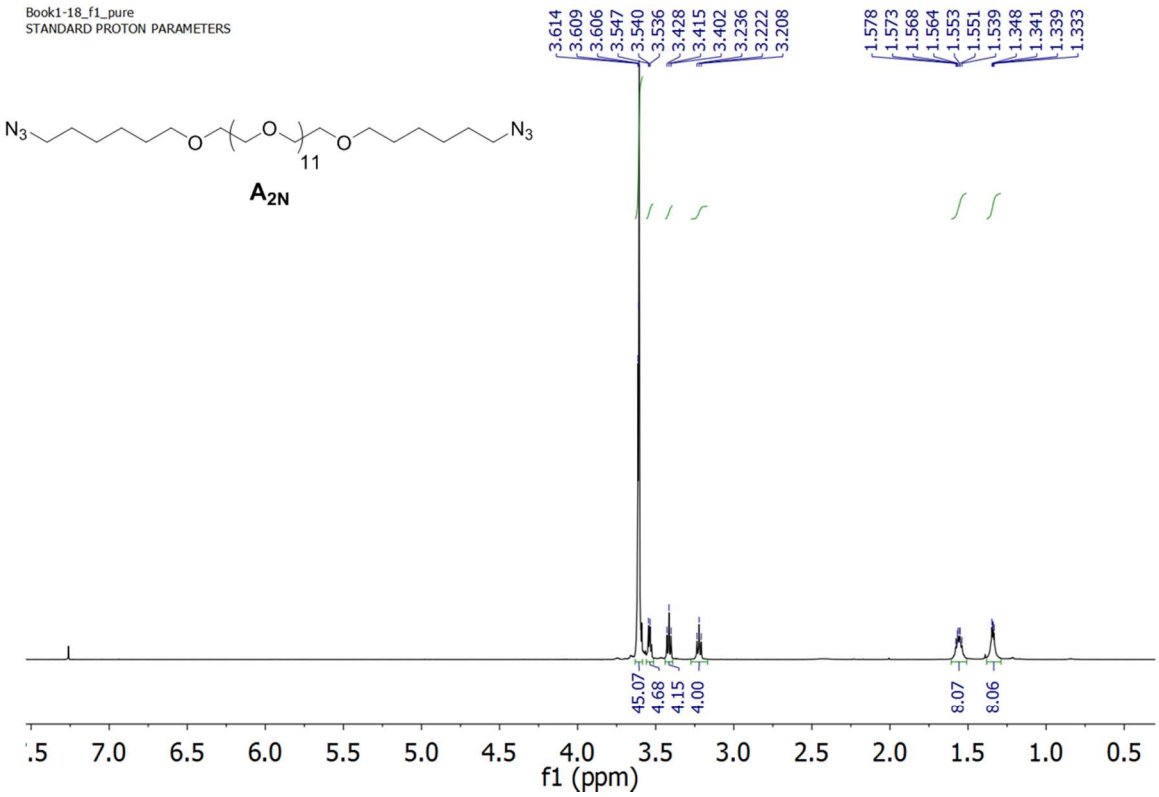

Figure S6. ^{1}H NMR (500 MHz, $CDCl_3$) for $\mathbf{A_{2N}}$ (PEG-12).

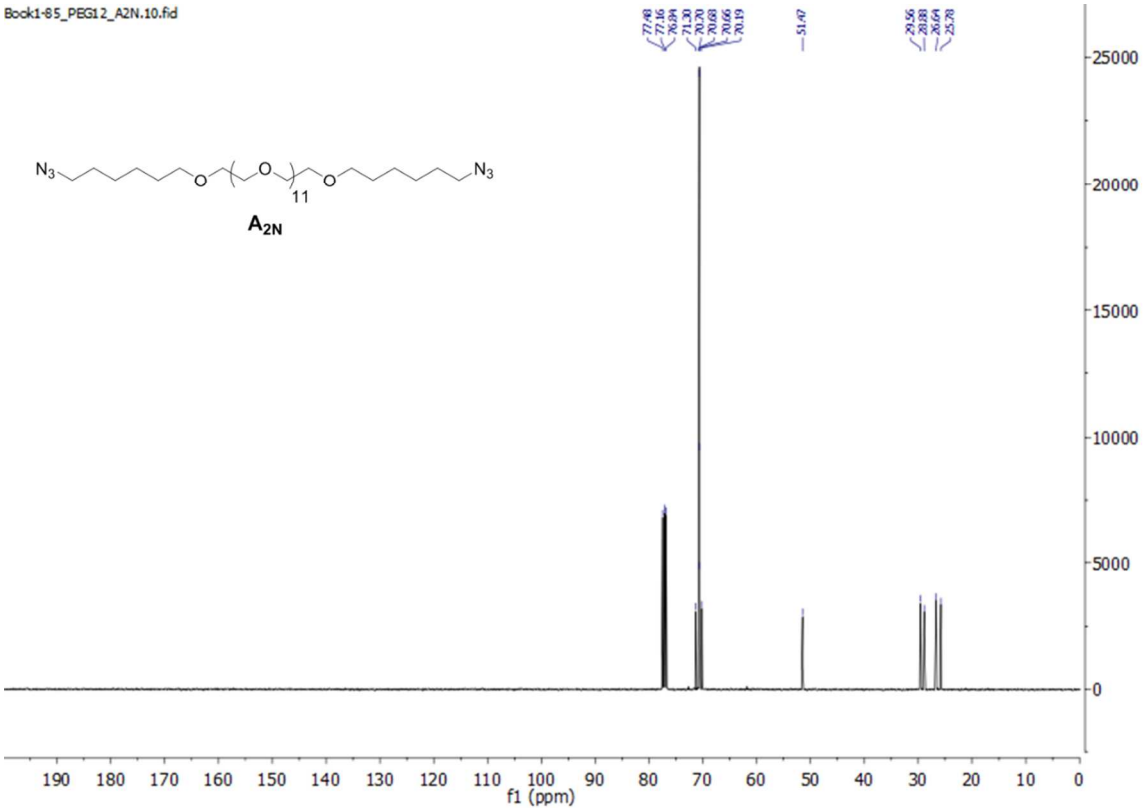

Figure S7. ^{13}C NMR (101 MHz, $CDCl_3$) for $\mathbf{A_{2N}}$ (PEG-12).

$\mathbf{A_{2H}}$ (PEG-28)

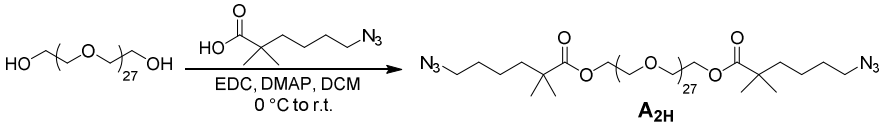

A_{2H} (PEG-28) was synthesized by using the similar procedure for $\mathbf{A_{2H}}$ (PEG-12) except that PEG-28 diol was used as the starting material. ^{1}H NMR (400 MHz, $CDCl_3$) δ 4.16 (d, J = 5.8 Hz, 4H), 3.71 – 3.45 (m, 108H), 3.21 (t, J = 6.9 Hz, 4H), 1.59 – 1.42 (m, 8H), 1.33 – 1.21 (m, 4H), 1.13 (s, 12H). ^{13}C NMR (101 MHz, $CDCl_3$) δ 177.61, 70.61, 70.59, 70.55, 69.15, 63.43, 51.20, 42.19, 40.02, 29.25, 25.11, 22.15. HRMS-ESI (m/z): calcd for $C_{72}H_{140}N_6O_{31}Na$ $[M+Na]^+$, 1607.9455; found, 1607.9484.

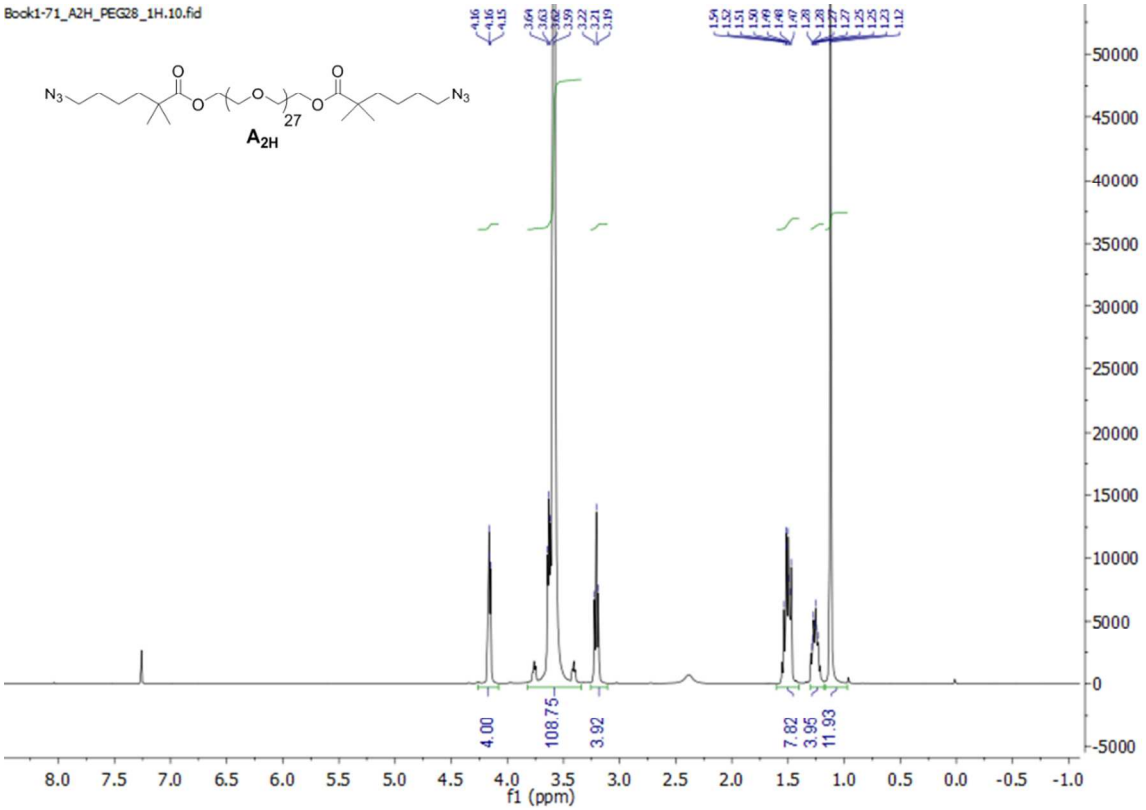

Figure S8. ^{1}H NMR (400 MHz, $CDCl_3$) for $\mathbf{A_{2H}}$ (PEG-28).

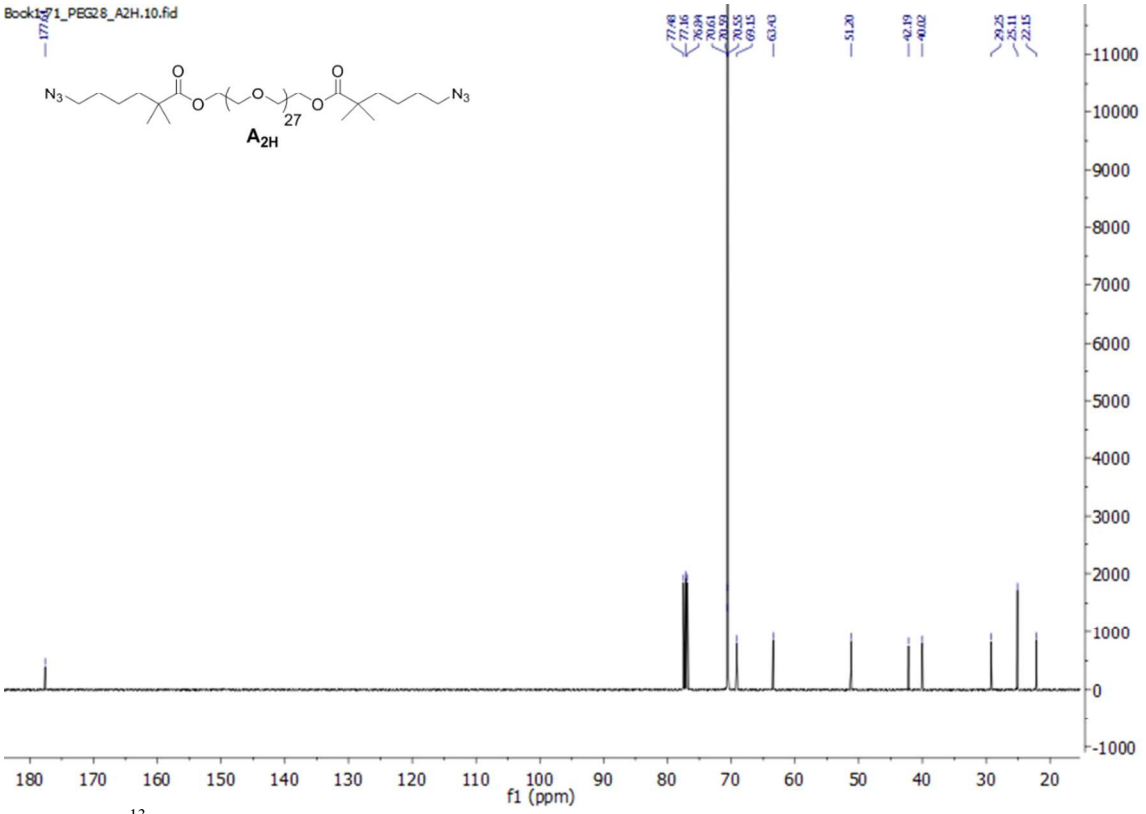

Figure S9. ^{13}C NMR (101 MHz, $CDCl_3$) for $\mathbf{A_{2H}}$ (PEG-28).

A_{2D} (PEG-28)

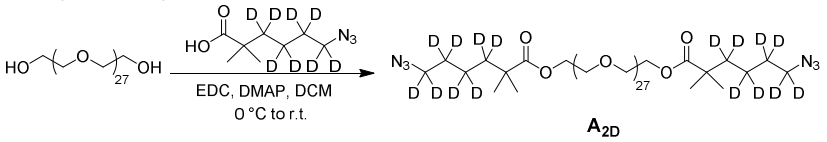

A_{2D}

A_{2D} (PEG-28) was synthesized by using the similar procedure for **A_{2D}** (PEG-12) except that PEG-28 diol was used as the starting material. ^{1}H NMR (400 MHz, $CDCl_3$) δ 4.19 (d, J = 5.6 Hz, 4H), 3.61 (d, J = 1.3 Hz, 108H), 1.14 (s, 12H). ^{13}C NMR (101 MHz, $CDCl_3$) δ 177.65, 77.40, 77.08, 76.76, 70.61, 70.59, 70.56, 70.54, 69.16, 63.42, 42.02, 25.05. HRMS-ESI (m/z): calcd for $C_{72}H_{124}D_{16}N_6O_{31}Na$ $[M+Na]^+$, 1624.0460; found, 1624.0481.

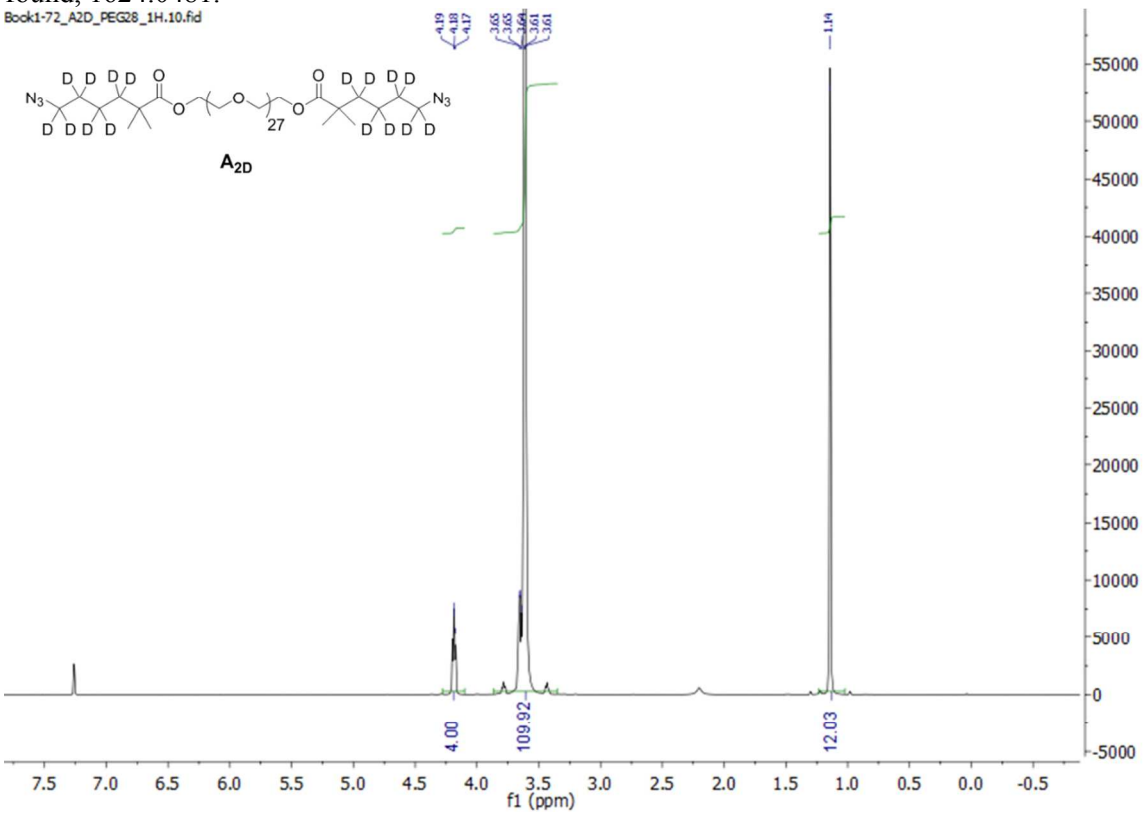

Figure S10. ^{1}H NMR (400 MHz, $CDCl_3$) for **A_{2D}** (PEG-28).

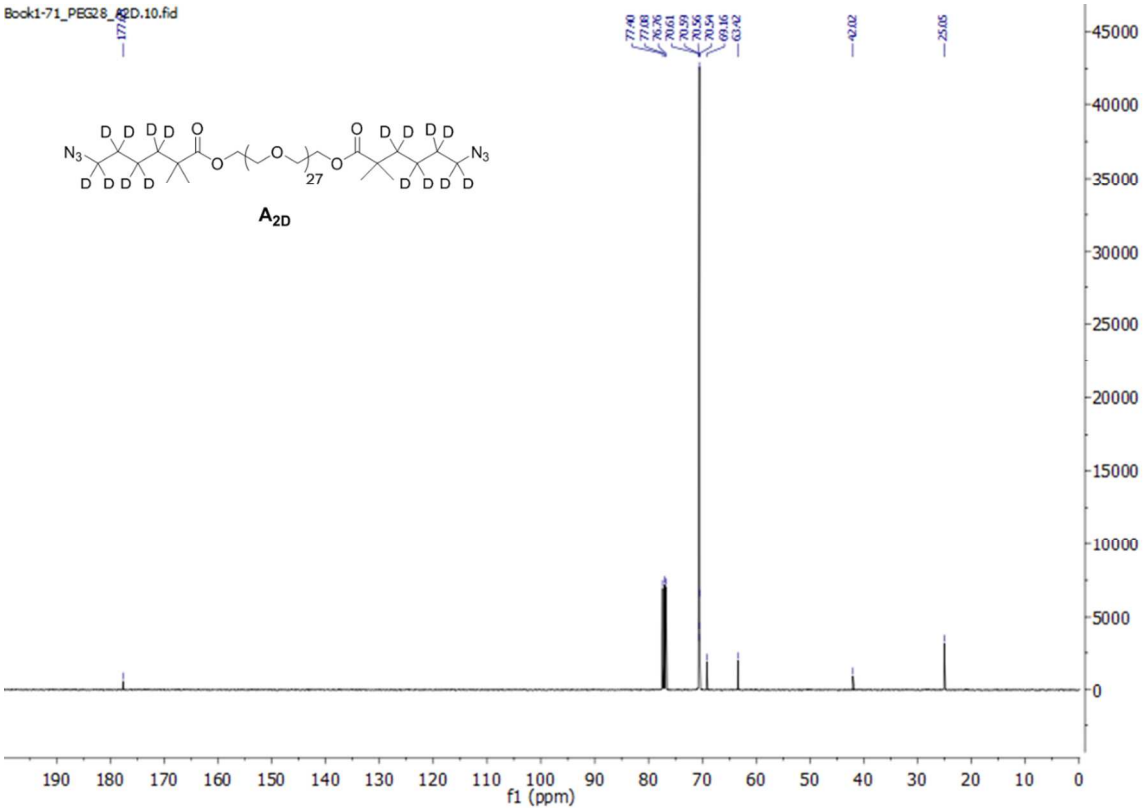

Figure S11. ^{13}C NMR (101 MHz, $CDCl_3$) for $\mathbf{A_{2D}}$ (PEG-28).

A_{2N} (PEG-28)

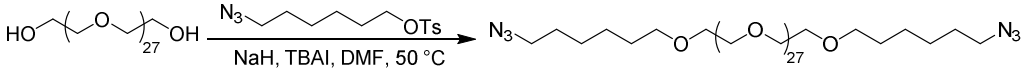

$\mathbf{A_{2N}}$

A_{2N} (PEG-28) was synthesized by using the similar procedure for $\mathbf{A_{2N}}$ (PEG-12) except that PEG-28 diol was used as the starting material. ^1H NMR (400 MHz, $CDCl_3$) δ 3.61 (m, 108H), 3.54 (t, J = 6.2 Hz, 4H), 3.42 (t, J = 6.6 Hz, 4H), 3.23 (t, J = 6.9 Hz, 4H), 1.64 – 1.45 (m, 8H), 1.42 – 1.19 (m, 8H). ^{13}C NMR (101 MHz, $CDCl_3$) δ 77.48, 77.16, 76.84, 71.28, 70.68, 70.64, 70.17, 51.45, 29.54, 28.86, 26.62, 25.76. HRMS-ESI (m/z): calcd for $C_{68}H_{136}N_6O_{29}Na$ $[M+Na]^+$, 1523.9244; found, 1523.9243.

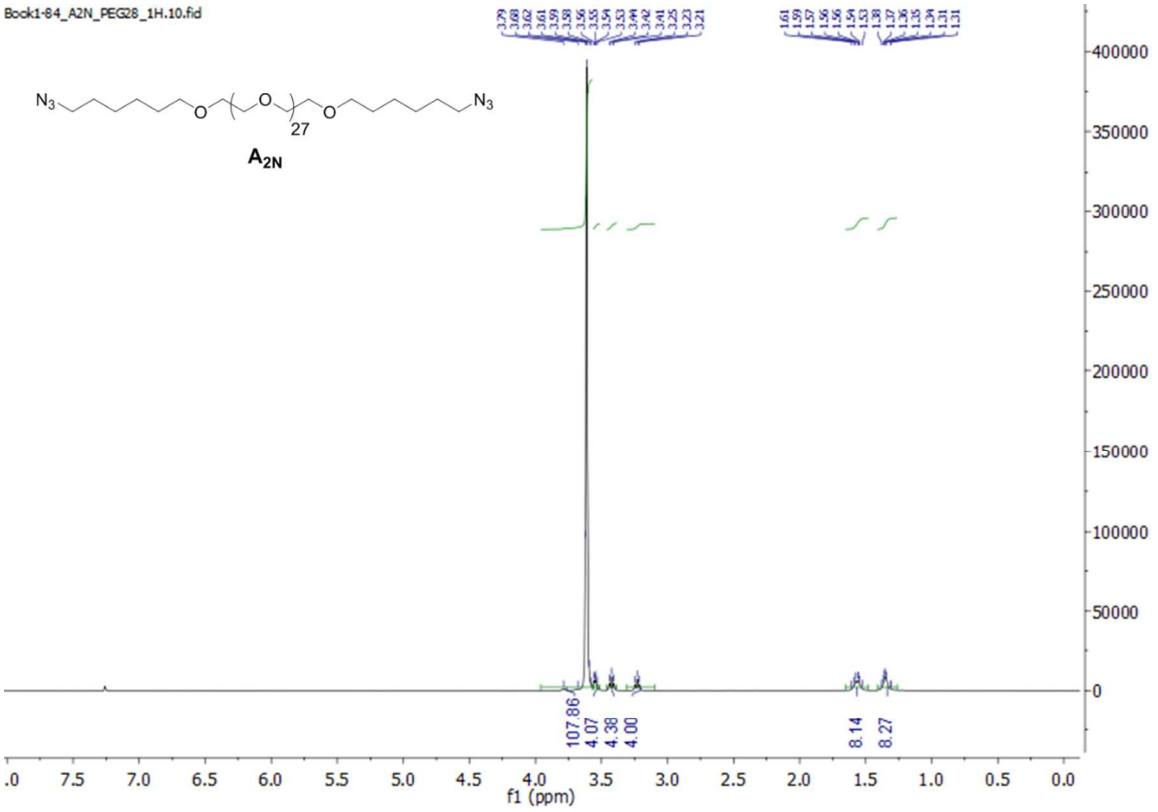

Figure S12. ^{1}H NMR (400 MHz, $CDCl_3$) for $\mathbf{A_{2N}}$ (PEG-28).

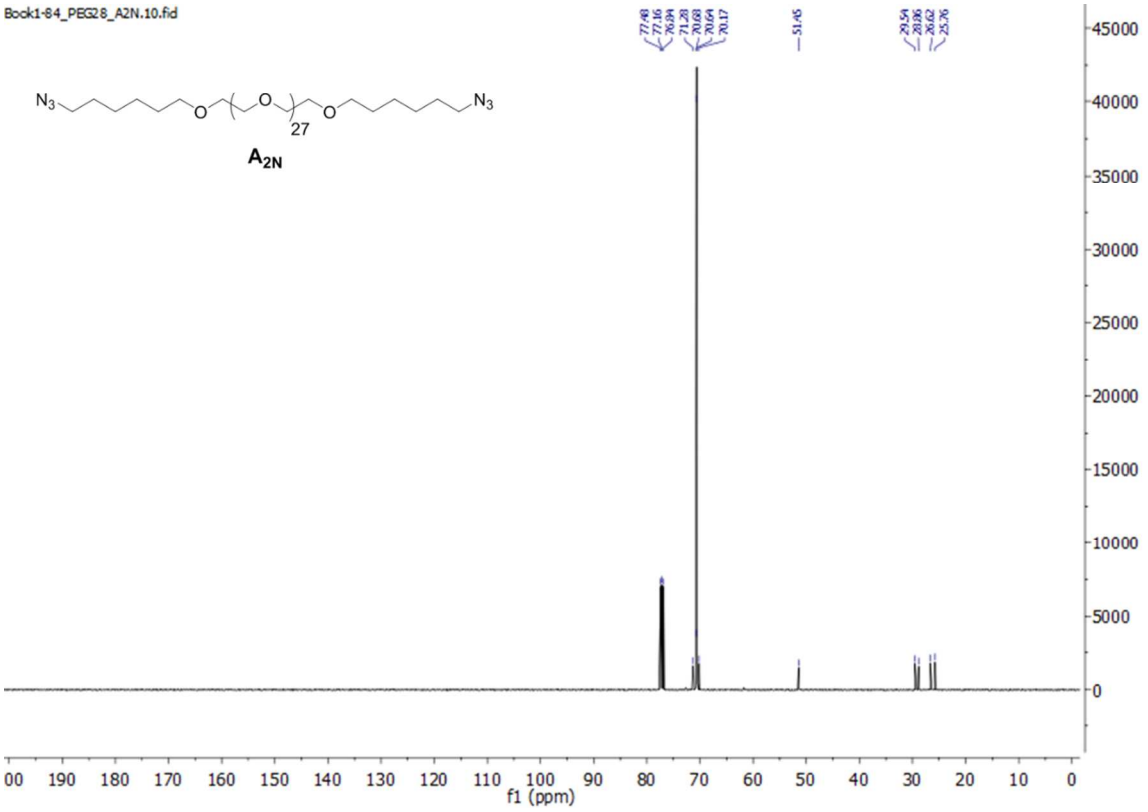

Figure S13. ^{13}C NMR (101 MHz, $CDCl_3$) for $\mathbf{A_{2N}}$ (PEG-28).

4. Preparation of the gels

$\mathbf{A_{2H}}$, $\mathbf{A_{2D}}$, $\mathbf{A_{2N}}$ and $\mathbf{B_3}$ were weighed in a 20 mL scintillation vial and transferred into a N_2-filled glovebox. In the glovebox, stock solutions of the monomers (200 mM $\mathbf{A_2}$, 90 mM $\mathbf{A_{2H}}$, 90 mM $\mathbf{A_{2D}}$, 20 mM $\mathbf{A_{2N}}$ and 133.3 mM $\mathbf{B_3}$) were prepared in CH_3CN in a volumetric flask. The stock solution of the mixture of CuBr and Me_6TREN (400 mM CuBr, 440 mM Me_6TREN) was made in CH_3CN was prepared in another vial. The preparation of the polymer networks was conducted in the glovebox, by sequentially adding CH_3CN, monomer solution and CuBr/Me_6TREN solution using a micropipette in 2 mL scintillation vials with white urethane solid cap. Upon the addition of starting materials, the vial was held on vortex mixer for 30 s to ensure homogeneous mixing. Different macromer concentrations (2 mM, 4 mM, 6 mM, 8 mM, 10 mM, 15 mM, 20 mM, 30 mM, 40 mM, 50 mM, 60 mM, 70 mM, 80 mM, 90 mM, 100 mM) were obtained by changing the amount of CH_3CN, monomer solution and CuBr/Me_6TREN, and 7 samples were made for each concentration. The samples were left for 24 h to ensure complete reaction.

5. Degradation of the gels

To degrade the networks, the samples were removed from the glovebox. The samples were then dissolved in 300 µL of 2 M KOH (aq) and vortexed. After >4 h of hydrolysis, the samples were analyzed via LC/MS.

6. Analysis of degradation products

The degradation products were analyzed by LC/MS using the Single Ion Mode (SIM) on the MS. The masses of junction types I (nnn, nni, nii, iii) and II (nnnn, nnni, nnii, niii, iiii) as well as incompletely reacted junctions were entered into the SIM, respectively, to identify the mass distributions of junction

types I, II and dangling chain ends resulted from incomplete reaction. The principal isotope peak for each degradation product was extracted in the "Extract Ion" feature of ChemStation, and quantified using the integration feature for each extracted ion.

7. Slow addition experiments

The slow addition experiments were performed similar to our previous work,[5] except that the reactions were conducted in a N_2-filled glovebox. A stock solution of the mixture of $\mathbf{A_2}$ (PEG-12) (200 mM, including 90 mM $\mathbf{A_{2H}}$, 90 mM $\mathbf{A_{2D}}$, 20 mM $\mathbf{A_{2N}}$), CuBr (440 mM) and Me_6TREN in CH_3CN was made in a volumetric flask. During slow addition experiments, certain volumes of the mixture solution of $\mathbf{A_2}$, CuBr and Me_6TREN were added into 2 mL autosampler vials with rubber septa and magnetic stir bar, and stoichiometric amount of $\mathbf{B_3}$ solutions were added to the mixture of $\mathbf{A_2}$, CuBr and Me_6TREN at a rate of 1 μL/min by using a KD-Scientific syringe pump. The solution was stirred during the addition. The macromer concentrations of networks were controlled by using changing the volumes of $\mathbf{A_2}$/CuBr/Me_6TREN solution and the concentrations and volumes of $\mathbf{B_3}$. Each slow addition experiments were repeated 3 times, and the corresponding batch mixing experiments were conducted 3 times as the control experiments. Table S2 shows the detailed volumes of $\mathbf{A_2}$/CuBr/Me_6TREN as well as the concentrations and volumes of $\mathbf{B_3}$ in order for different macromer concentrations of networks. In case of the 60 mM sample, since gelation occurred, 70 μL of $\mathbf{B_3}$ was added at a rate of 1 μL/min and the other half was added to the solution in one shot. In our previous work, we have demonstrated that the rate of addition impacted the primary loop fraction, and the decrease of the addition rate led to less primary loop fraction; but once the addition rate was below a critical value u*, the primary loop fraction did not decrease any more and reached the minimum.[5] According to our derivation, $u^* = 0.01kV_0[A_2]$, where k is the second-order rate constant of the reaction, V_0 is total volume of $[B_3]$ solution to be added, and $[A_2]$ is the concentration of $[A_2]$. $k = 0.02\ M^{-1}s^{-1}$,[6] $V_0 = 200$ μL, $[A_2] = 200$ mM, $u^* = 2.4$ μL/min. Since the rate of slow addition that we set up was 1 μL/min, lower than the critical value u*, we should obtain the minimized loop defects.

Table S2. The detailed volumes of $\mathbf{A_2}$/CuBr/Me_6TREN as well as the concentrations and volumes of $\mathbf{B_3}$ that were used to make the networks.

Macromer concentration of network (mM)	V ($\mathbf{A_2}$/CuBr/Me_6TREN) (μL)	c ($\mathbf{B_3}$) (mM)	V ($\mathbf{B_3}$) (μL)
10	10	7.02	190
20	20	14.81	180
40	40	33.3	160
60	60	57.14	140

8. Rheometry

The gel samples (300 μL in total) for rheometry were prepared in DMSO in 4 mL vials, which were broken with a hammer before the gels were transferred out. The gels were subsequently cut with an 8 mm hole puncher (purchased from McMaster-Carr), and transferred onto the rheometer. Experiments were performed at 25 °C and the evaporation of DMSO was negligible within the typical measurement time (< 20 minutes). The rheology testing was performed on a TA Instruments Discovery Hybrid Rheometer HR-2 rheometer, with an 8 mm standard parallel steel plate geometry. The measurements were performed at 25 °C. A strain sweep was performed to determine a linear viscoelastic region for frequency sweep

studies. A frequency sweep was then performed from 0.1 Hz to 10 Hz at a constant strain of 0.5%. Shear modulus G' was determined based on G' values at 1 rad/s. The detailed rheological data are shown in Figure S14.

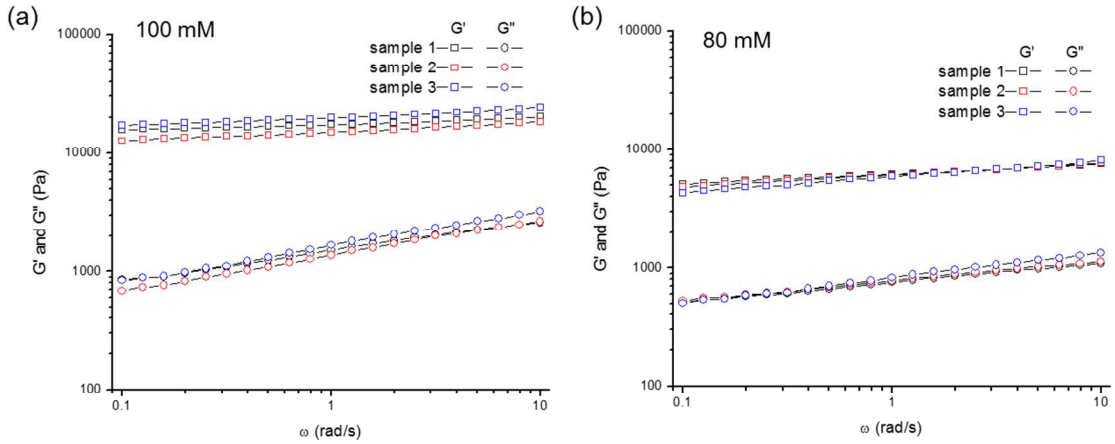

Figure S14. Rheological data of A_2 + B_3 gels with different initial concentrations of **A_2** macromonomer: (a) 100 mM; (b) 80 mM. (T = 25 °C, shear strain = 0.5%)

9. Rate theory

In this study, the experimentally measured loop fractions of A_2+B_3 end-linked gels are compared to the rate theory predictions calculated by the kinetic graph theory. The kinetic graph theory (KGT) is a modified rate theory that tracks the kinetics of the formation of infinitely large network through a set of differential equations describing interconversion between a series of finite subgraphs. Each functional group on a subgraph junction may be unreacted, contain a dangling chain, contain a looped chain, or be connected to the underlying network through a bridging chain. The junctions are assumed to be uncorrelated beyond a critical size, and cyclic topologies are recorded. For functional groups belonging to different subgraphs, the rate of formation of the bridging connection (intermolecular reaction) is modelled with second order kinetics

$$R_{ij,\text{bridge}} = k_{AB}[A_i][B_j] \quad \text{(Eq. S8)}$$

where k_{AB} is the second order rate constant, and $[A_i]$ and $[B_j]$ are the instantaneous concentrations of A and B functional groups on species i and j, respectively. For groups belonging to the same subgraph, the rate of reaction depends on the probability of two unreacted functional groups encountering each other. Modelling A_2 precursors as Gaussian chains with mean square end-to-end distance $\langle R^2 \rangle$, the probability of two functional groups separated by n chains encountering each other is $P_n = (3/2\pi n\langle R^2 \rangle)^{3/2}$. Hence, the reaction rate for groups belonging to the same subgraph (intramolecular reaction) is

$$R_{i,\text{loop}} = k_{AB} \frac{N_{A,i}^n}{N_{\text{Av}}} \left(\frac{3}{2\pi n\langle R^2 \rangle}\right)^{3/2} [B_i] \quad \text{(Eq. S9)}$$

where $N_{A,i}^n$ is the number of functional group A contained in subgraph i which can form the n^{th}-order loop, and N_{Av} is Avogadro's number.

Previous reports[1,6] have demonstrated that a two junction rate theory (KGT with critical size of two junctions) can give an accurate description of primary loop fractions. However, the two junction theory overestimates secondary loop fractions in the neighborhood of the maximum. In order to accurately capture secondary loops, a higher order rate theory is needed. In this study, KGT is extended beyond the

original two junction theory to a "2.5 junction" theory. Unlike the original two junction theory, where only one type of bridging connection to the network is considered, in the 2.5 junction theory, the exact types of bridging connections between the junction and the underlying network are explicitly considered. For a junction that has x connections to the underlying network, there are P_x different types of connections to the network, where P_x is the number of unrestricted partitions of integer x. For example, a trifunctional junction with two connections to the network has $P_2 = 2$ possible types of connections to the network, representing the case where the two strands connect to the same junction or to two distinct junctions, whereas a junction with only one connection to the network has $P_1 = 1$ possible type of connection. This extension enables the explicit consideration of all possible local connectivity structure that a multifunctional junction can have. At this level of approximation, there are a total of 50 subgraphs, 1304 bridging reactions, and 22 looping reactions. A complete schematic illustration of the 50 subgraphs considered in the formation of A_2+B_3 network is shown in Figure S15.

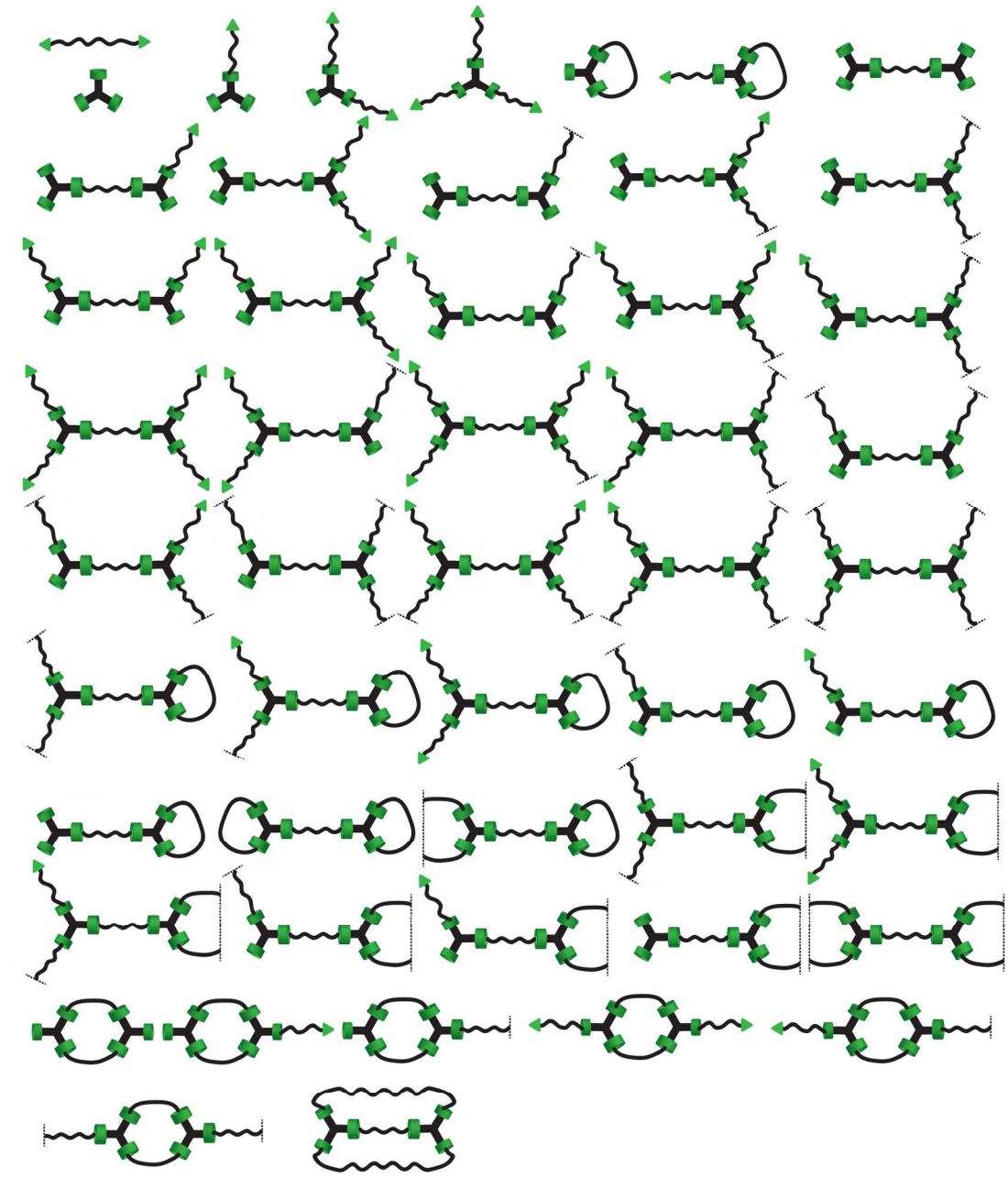

Figure S15. KGT subgraphs for 2.5 junction theory. Dashed lines indicate the cutoff of a connection to the underlying network. Multiple arms connected to the same dashed line represents the connection of multiple arms to the same junction in the network.

10. References

1. Zhou, H.; Woo, J.; Cok, A. M.; Wang, M.; Olsen, B. D.; Johnson, J. A., *Proc. Natl. Acad. Sci. U. S. A.* **2012,** *109* (47), 19119-19124.
2. Zhou, H. X.; Schon, E. M.; Wang, M. Z.; Glassman, M. J.; Liu, J.; Zhong, M. J.; Diaz, D. D.; Olsen, B. D.; Johnson, J. A., *J. Am. Chem. Soc.* **2014,** *136* (26), 9464-9470.
3. Kawamoto, K.; Zhong, M.; Wang, R.; Olsen, B. D.; Johnson, J. A., *Macromolecules* **2015,** *48* (24), 8980-8988.
4. Goldup, S. M.; Leigh, D. A.; Long, T.; McGonigal, P. R.; Symes, M. D.; Wu, J., *J. Am. Chem. Soc.* **2009,** *131* (43), 15924-15929.

5. Gu, Y.; Kawamoto, K.; Zhong, M.; Chen, M.; Hore, M. J. A.; Jordan, A. M.; Korley, L. T. J.; Olsen, B. D.; Johnson, J. A., *Proc. Natl. Acad. Sci. U. S. A.* **2017,** *114* (19), 4875-4880.
6. Jia, Z.; Bell, C. A.; Monteiro, M. J., *Chem. Commun.* **2011,** *47* (14), 4165-4167.